www.czasopisma.pan.pl PAN POLSKA AKADEMIA NAUK www.journals.pan.pl

Arch. Min. Sci. **68** (2023), 2, 335-350

Electronic version (in color) of this paper is available: http://mining.archives.pl

DOI: https://doi.org/10.24425/ams.2023.146183

JIANG YAO[1], YINBO XUE[2*], XIAOLIANG LI[2], LEI ZHAI[2], ZHENYU YANG[3], WENHUI ZHANG[3]

MACHINE VISION ONLINE DETECTION OF ORE GRANULARITY BASED ON EDGE COMPUTING

Belts are widely applied in mine production for conveying ores. Understanding ore granularity, which is a crucial factor in determining the effectiveness of crushers, is vital for optimising production efficiency throughout the crushing process and ensuring the success of subsequent operations. Based on edge computing technology, an online detection method is investigated to rapidly and accurately obtain ore granularity information on high-speed conveyor belts. The detection system utilising machine vision technology is designed in this paper. The high-speed camera set above the belt is used to collect the image of the ore flow, and the collected image is input into the edge computing device. After binary, grey morphology and convex hull algorithm processing, the particle size distribution of ore is obtained by statistical analysis. Finally, a 5G router is used to output the settlement result to a cloud platform. In the GUANBAOSHAN mine of Ansteel Group, the deviation between manual screening and image particle size analysis was studied. Experimental results show that the proposed method can detect the ore granularity, ore flow width and ore flow terminal in real-time. It can provide a reference for the staff to adjust the parameters of the crushing equipment, reduce the mechanical loss and the energy consumption of the equipment, improve the efficiency of crushing operation and reduce the failure rate of the crusher.

Keywords: Ore granularity; Machine vision; Online detection; Edge computing

1. Introduction

In mine crushing production, the information on ore particle size distribution is an index reflecting the crushing effect. By detecting the size distribution of ore particles, we can ensure

[1] NORTHEASTERN UNIVERSITY, CHINA
[2] CHINESE ACADEMY OF SCIENCES ALLWIN TECHNOLOGY CO., LTD, CHINA
[3] ANSTEEL GROUP GUANBAOSHAN MINING CO., LTD, CHINA

* Corresponding Author: Xueyinbo@zkaw.com.cn

that particle size requirements are met and optimise the ore-feeding process by adjusting the crusher's parameters. This leads to improved ore dressing efficiency, reduced energy consumption, and significant economic benefits for mine production. Meanwhile, the change in the monitored data can also help diagnose the equipment fault. For example, if the monitoring data of ore particle size distribution changes drastically, it implies that the vibrating screen may be damaged. If there is no ore on the belt, it indicates that the ore drawing funnel may be blocked. Therefore, the identification of ore granularity is a significant research topic for the mining industry. Due to the difficulty in the existing ore particle size detection technology, the crushing process is most often controlled manually in most mines. Traditional ore particle size detection mostly uses manual offline screening, and the detected ore particle size information lags. Even if artificial video monitoring devices are adopted to tell whether the ore flow is normal, there are still missing reports during the night shifts in the production process.

The traditional detection of ore particle size distribution mainly uses manual or mechanical devices, and sieves of different sizes in turn. For example, the sieves with different screen sizes are used to ensure that the ores pass gradually and in different grades through screens in accordance with the ore particle size distribution. However, this method requires many sieves and involves many procedures. In addition, the shape of the screen and human factors can impact the accuracy of the detection results.

With the development of artificial intelligence (AI) technology, AI technology has been applied in increasing fields to do jobs which can only be carried out manually. Ma et al. [1] used machine vision (MV) and image processing technology to detect ore size and calculate the particle size distribution. Chen et al. [2] realised the classification of rock discontinuity trajectories based on machine learning (ML) of image samples. Li et al. [3] used MV to detect belt tear based on a line laser. Song et al. [4] used the digital speckle correlation method to calculate image data collected by a charge-coupled device (CCD) camera. Zhou et al. [5] proposed a new MV method to measure tool wear. Habib et al. [6] proposed papaya disease recognition based on MV. Liu et al. [7] proposed online PCB defect detection based on MV. Eshaq et al. [8] used MV and convolution neural networks (CNN) for deep learning (DL) to distinguish coal quality. Guo et al. [9] proposed a chicken floor distribution monitoring method based on MV. Tian et al. [10] used MV technology to detect surface defects of stamping and grinding flat parts. Hafiz Muhammad et al. [11] established a model for estimating Q-factor and elastic modulus based on AI. Baduge et al. [12] summarised the application of AI, ML and DL in architecture design and visualisation in architecture and architecture 4.0, and also introduced the trends and possible research approaches in these fields. AI technologies have been applied in various industries with remarkable results.

Accurate measurement of ore particle dimensions is crucial for mining, and MV is the tool that provides this measurement. Bhondayi [13] summarised the measurement methods of foam phase bubble size in mineral foam flotation and proposed that the flotation foam size can be analysed based on MV. Maitre et al. [14] proposed mineral grains recognition with MV and ML. Lu et al. [15] separated the particles from each other with standard morphological operations, such as swelling and corrosion. Laucka et al. [16] proposed a method of measuring fertiliser particle size distribution based on image processing, which used morphological operators to find the contour of the particles. Zhang et al. [17] established and tested an online MV system to predict the ash content of coal products on the belt. Martins Gomes et al. [18] proposed a method to automatically measure and classify Hematite crystals in iron ore based on texture features. Heyduk [19] proposed an approximation method of the particle contour that can be applied to MV systems for

particle size distribution analysis. It is believed that MV will see an even wider application in mine production.

Edge computing (EC) involves utilising IoT edge devices for collecting data and performing intelligent analysis and calculations. This enables intelligent flow between the cloud and the edge. It has been studied and even applied in many enterprises and by many researchers. Thakur et al. [20] realised that smart water conservation was possible through machine learning and blockchain-distributed EC network. Aazam et al. [21] proposed task unloading in intelligent medical EC based on ML. Rajavel et al. [22] proposed an intelligent medical video monitoring system of IoT based on EC. Gawas et al. [23] proposed security data sharing and integration method of vehicle EC based on blockchain. In the future, EC technology will witness an even wider application in industry.

For the above methods or systems based on the MV technique, many problems still need to be solved, and the techniques need to be optimised for better application. For example, due to the high speed of the ore conveyor belt before the magnetic grinding process (the average speed is 2.5 m/s), the image collected by ordinary MV equipment can be very blurred due to the latency. As water is most often required in the previous crushing process, the ore particles usually are quite adhesive, resulting in variances in particle sizes, which leads to the problems of low accuracy of particle size analysis, ineffective separation of adhesion particles and excessive separation of adhesion particles. At present, the accuracy of recognising ore particle size less than 12 mm is relatively low, while the feed particle size of the magnetic grinding process in most concentrators is less than 12 mm in practice.

To solve the above technical problems, this paper combines MV technology, EC technology and IoT technology to solve the problem of small particle recognition on a high-speed belt, triggering the alarm of abnormal particle size data and ore flow terminal. After binary, grey morphology and convex hull algorithm processing, the particle size distribution of ore is obtained by statistical analysis. Finally, a 5G router is used to output the settlement result to the IoT server by message queuing telemetry transport (MQTT) protocol. The user can then view the real-time and historical data of ore granularity and ore flow width through a web server. Experimental results show that the proposed method can detect the ore grading information after crushing in real-time, provide a reference for the staff to adjust the parameters of the crushing equipment, reduce the mechanical loss and the energy consumption of the equipment, improve the efficiency of crushing operation and reduce the failure rate of the crusher.

2. Composition of Ore Granularity Detection

2.1. System Structure of Ore Granularity Detection

Fig. 1 shows the structure of the ore granularity detection system. The hardware components include a CCD industrial camera, light source, bracket, EC device, 5G router, and other accessory parts. The CCD industrial camera collects the image of the ore flow on the belt and inputs the collected image into the EC device.

When the ore is transported on the belt, its image features a bulge in the middle, and two light sources are configured for light intensity. The bracket is made of a 4040c industrial aluminium profile, the shape of which is a goal structure. The crossbeam part can move up and down to adjust the distance between the high-speed camera and ore flow. The camera and light

source is installed on the crossbeam and can move left and right to obtain the best shooting angle and lighting. The EC device is used to process the ore flow image and output the calculated ore particle size distribution result through the serial port of the EC device and transmit it to the 5G router. The 5G router is used to transmit the calculated ore particle size distribution results to the IoT server on the cloud platform through the 5G wireless network. It transmits the data with the MQTT protocol of the IoT for data visualisation display.

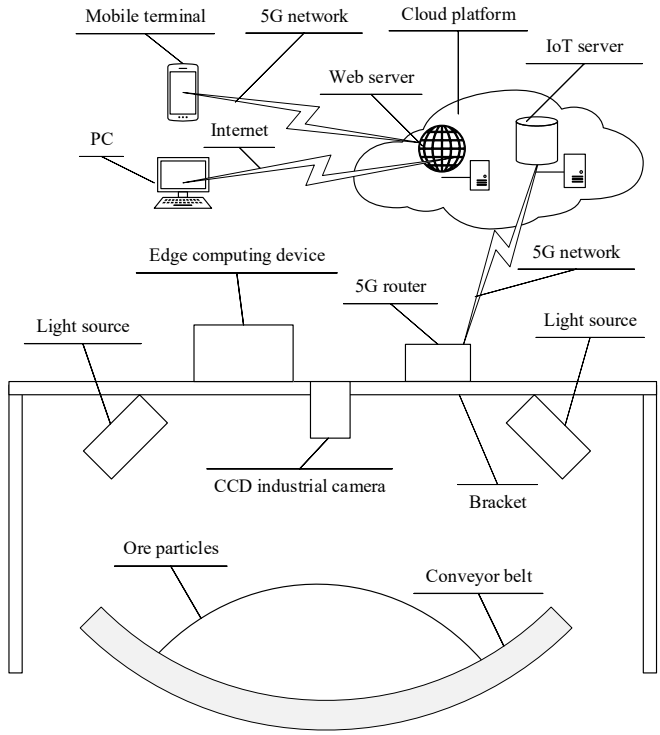

Fig. 1. Composition of hardware equipment for detecting ore granularity

A web server and IoT server are deployed on the cloud platform. The IoT server is employed for receiving and storing the data sent by the 5G router, and the web server for publishing web services. Mobile terminals can use a 5G network, and a PC can use the Internet to access web services on a cloud platform and view real-time data and historical data of ore granularity data, as shown in Fig. 2. The title in the upper part of the figure shows that the position of the image acquisition is 1# belt at the Milling and Magnetic Separation (MMS) entrance and the image acquisition frequency is once every 10 seconds. Next, two images are displayed, the left is the original image obtained by the camera, and the right is the processed result. In the lower part, the information on the image acquisition time, proportion of large blocks and width of ore flow is displayed below. The lower half of the graph shows the real-time and historical data on the proportion of large blocks and the width of the ore flow. The title is “real-time data” and “frequency: 10 seconds”. Next, acquisition time, proportion of large blocks and width of ore flow information

are displayed. At the lower part, the curve of the current day's bulk ratio and the data for ore flow width is displayed by default. Historical data can be viewed by clicking the "<" or ">" button.

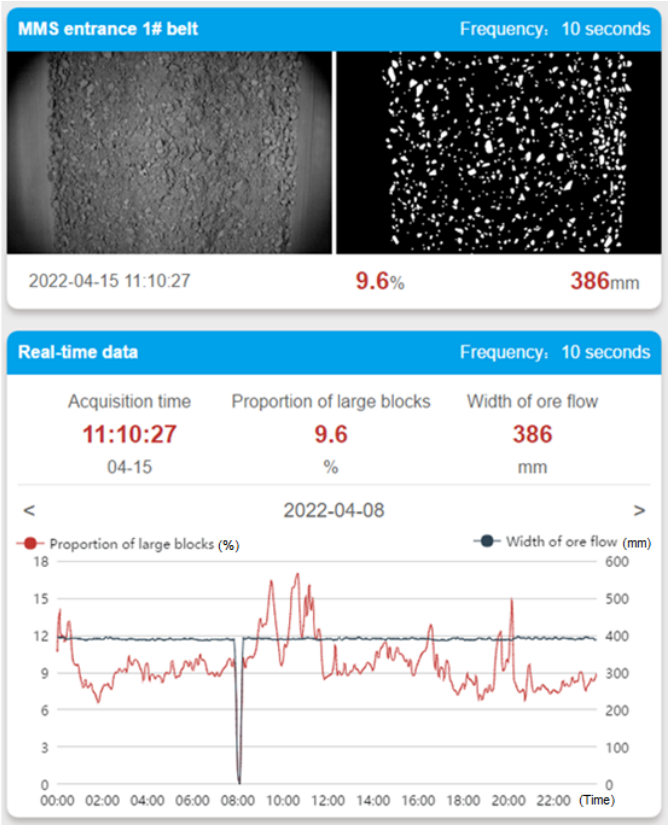

Fig. 2. Ore granularity data display page

2.2. The Flow Diagram of Ore Granularity Detection

The flow diagram of ore granularity detection is presented in Fig. 3.

The ore granularity detection can be divided into two processes: image process and abnormal condition detection. To begin the image processing, we acquire the original image using a CCD industrial camera. Secondly, binary processing, grey morphology processing and convex hull algorithm are carried out, respectively. Lastly, the particle size distribution of ore is obtained by statistical analysis. Abnormal conditions are detected by analysing the ore granularity data to determine if there is any interruption in the flow of the ore. When the total number of ore particles is less than 200, the ore flow is considered to be interrupted. If there is any interruption in the flow of ore, an alarm will sound, and a determination will be made regarding the completion of the process. To determine if the screen is damaged, observe the average particle size changes within 5 minutes when the ore flow is normal. If the screen changes more than twice in 5 minutes, we

will conclude that it is damaged and an alarm will sound. We will then decide whether to stop the process entirely. The decision to either end the entire process or begin acquiring the next image will be based on whether the processing has been completed or not.

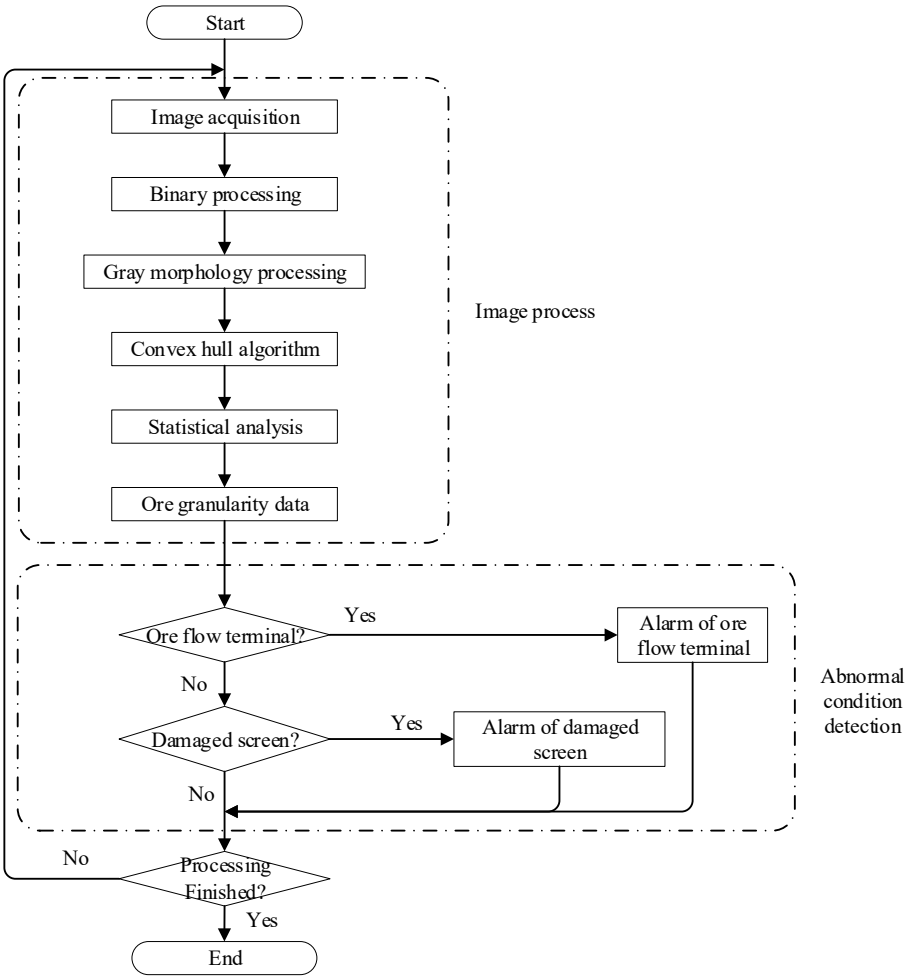

Fig. 3. The flow diagram of ore granularity detection

3. Ore Flow Image Acquisition and Processing

Scholars from various countries have done a lot of research on the operations of images. Li et al. [24] measured the binary fluidisation of nonspherical and spherical particles using machine learning-aided image processing. Jia [25] realised the application of binary images in building elevation design and found a method of building elevation based on the characteristics of binary images, and K. Tartarotti Nepomuceno Duarte et al. [26] realised that brain extraction in multi-

ple T1-weighted magnetic resonance imaging slices using digital image processing techniques. Chéles et al. [27] developed an image-processing protocol using well-established techniques to segment the image of blastocysts and extracted variables of interest.

As shown in Fig. 1, the CCD industrial camera is vertically installed above the ore conveyor belt. The image of ore particles on the conveyor belt is converted into a digital image by a camera, and the image data is sent to the EC device. By adjusting the focal length of the camera lens, the clarity of the image can be ensured. To ensure the brightness of the image, adjust the aperture of the camera lens. The camera is directly connected to the EC device, and the image acquisition program written by JAVA and LabVIEW image processing program is used to realise the online image acquisition and processing. Through system processing, the image of each stage in the image-processing process can be acquired.

3.1. Ore Flow Image Acquisition

Due to the exposure time of the camera being set as 2 ms, the captured image is dark, so it is necessary to adjust the brightness of the image using the algorithm.

$$y = (a \cdot x + b)^g \tag{1}$$

Where x is the source image pixel, y is the output image pixel, and the brightness b is set as 255 and the contrast a 73.00. The gamma value g is 0.30, and the processing result is shown in Fig. 4(a).

3.2. Ore Flow Image Binary Processing

For image binarisation, the background correction threshold method is used to obtain the threshold value. If the grey value of a pixel in the image is less than the threshold value, the grey value of the pixel is set as 0, otherwise, the grey value is set as 255 using the expression.

$$f(x) = \{0,\ x < T\ 255,\ x \geq T \tag{2}$$

Where T is the threshold, and the processing results are shown in Fig. 4(b). In this paper, T is set as 200.

3.3. Ore Flow Image Grey Morphology Processing

The image is processed by grey morphology using the expression

$$A \oplus B = \left\{ z \mid \left(\hat{B} \right)_z \cap A \neq \varnothing \right\} \tag{3}$$

After expansion treatment, the formula is as follows

$$A \odot B = \left\{ z \mid (B)_z \subseteq A \right\} \tag{4}$$

Corrosion treatment, namely open objects operation treatment, is used to remove the bright spots in the dark area, and 9 * 9 convolution cores are set. The processing results are shown in Fig. 4(c).

(a) The original image

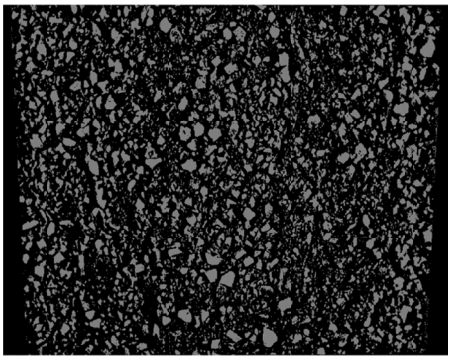

(b) Binary processing graph

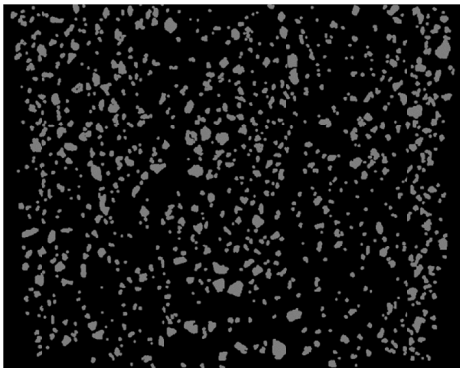

(c) Grey morphology processing graph

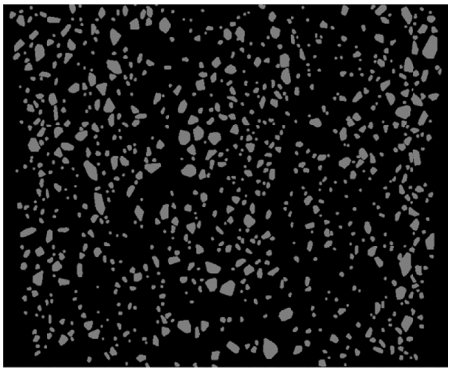

(d) Convex hull algorithm graph

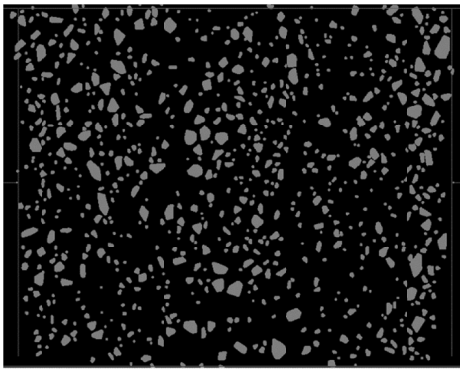

(e) Clamp processing

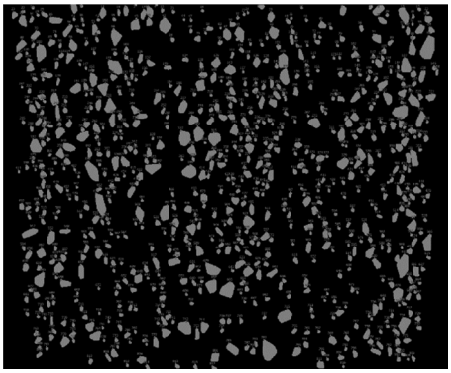

(f) Measurement results

Fig. 4. Ore flow image processing graph

3.4. Ore Flow Image Convex Hull Algorithm

A convex hull algorithm is applied to mark the contour of the ore in the image. The processing results are shown in Fig. 4(d).

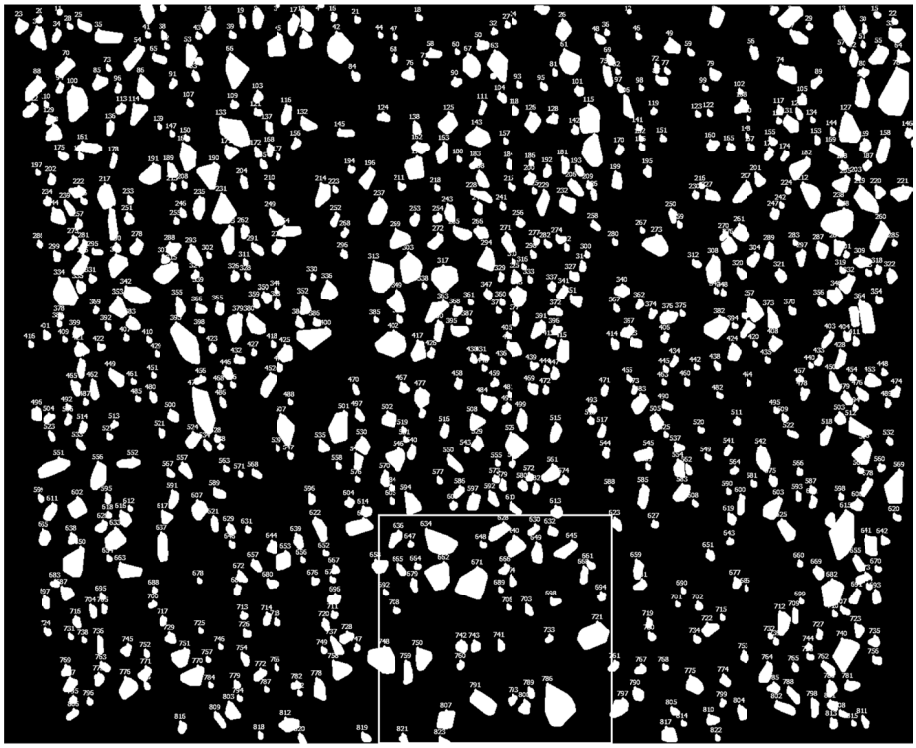

Fig. 5. Enlarged picture of measurement results

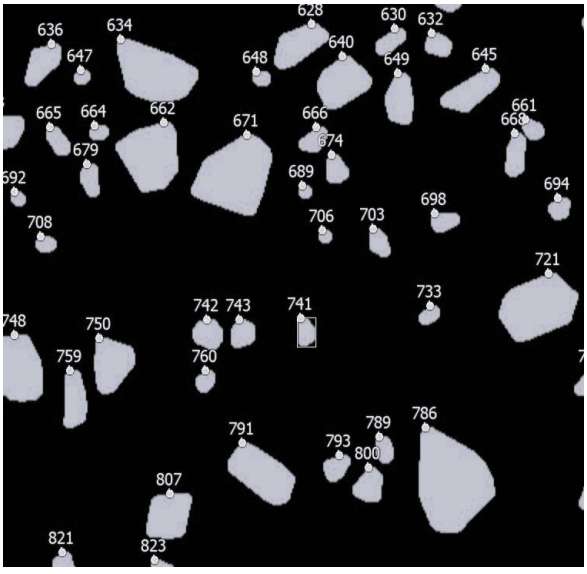

Fig. 6. Partial Enlarged Picture

3.5. Ore Flow Image Clamp Processing

Find edges along a rectangular region of interest shown in the image and measure the distance between the first and the last edges found. The processing results are shown in Fig. 4(e).

3.6. Ore Granularity Statistical Analysis

Traverse all the ore particles on the image, get the length, width and area of each ore particle, and calculate the ore particle size distribution. The processing results are shown in Fig. 4(f).

An enlarged picture of measurement results is shown in Fig. 5. As can be seen from the figure, a total of 823 ore particles have been identified.

Fig. 6 is a partially enlarged picture of the box in Fig. 5. As can be seen from Fig. 6, each ore particle is numbered. Table 1 is the summary data of the number and area of ore particles shown in Fig. 6. The unit of area is a pixel. From Table 1, we can see that the largest particle is 786, with an area of 2450 pixels, while the smallest particles are 689 and 706, with an area of only 69.

TABLE 1

Ore particle number and area data

Object No.	Area (pixels)	Object No.	Area (pixels)	Object No.	Area (pixels)	Object No.	Area (pixels)	Object No.	Area (pixels)
628	666	649	511	679	225	733	134	789	181
630	230	661	161	689	69	741	192	791	1093
632	226	662	1352	692	82	742	318	793	234
634	1512	664	112	694	176	743	251	800	343
636	441	665	215	698	203	748	1573	807	746
640	845	666	226	703	204	750	743	821	177
645	624	668	322	706	69	759	485	823	142
647	91	671	1903	708	128	760	151		
648	105	674	228	721	1601	786	2450		

4. Statistics and Comparison of Ore Sampling Results

The ore particle size distribution data obtained above is only the 2D data of the surface, and the 3D distribution data of the corresponding region should be inferred. At the same time, these data are all in pixels, and the pixel results are varied in accordance with the distance between the camera and the ore flow surface. As a scraper is installed at the belt feeding opening, the feed homogeneity is ensured, and the surface shape of the ore flow is unified, making the analysis results more representative.

The unit pixel of ore in the image is related to the actual unit size of it, and they are proportional. Therefore, by adopting a fixed appropriate proportion, the pixel data of the ore image can be converted into the actual particle size of the ore. After the actual measurement on-site, 1 mm is equivalent to 3.62 pixels. In the calculation, the sum of the area of particles with a length or width greater than 12 mm is taken as the numerator, and the identified ore flow area is taken as the denominator, the result is the distribution of ore particles.

As shown in Fig. 2, it can be seen from the image that about 9.6% of the ore particles are larger than 12 mm. The result of the image processing and analysis system for ore size and the result of manual screening is verified by converting pixel values to actual sizes, which is designed to test whether the system can be applied in the actual production.

The following is an example of a mine to study the error between manual screening and ore granularity detection system. Sieves were used to divide the ore into 2 particle size ranges: 0 mm ~ 12 mm, over 12 mm. The error of 15 sampling statistics is shown in Table 2.

TABLE 2

Comparison of sampling data

No.	Manual screening			Ore size analysis			
	Screening quality (kg)	Total weight (kg)	Screening production (PA), (%)	Sum of area of particles >12 mm (mm^2)	Ore flow area (mm^2)	Detection system (PV), (%)	Error (|PA-PV|) (%)
1	3.90	78.00	5.00	9643	125231	7.70	2.70
2	5.85	77.30	7.57	9702	126000	7.70	0.13
3	3.90	55.00	7.09	9175	127431	7.20	0.11
4	4.10	54.00	7.59	9649	128647	7.50	0.09
5	6.05	70.80	8.55	10227	127834	8.00	0.55
6	5.50	68.00	8.09	10392	126733	8.20	0.11
7	3.70	56.00	6.61	8466	126357	6.70	0.09
8	4.75	70.20	6.77	9518	125236	7.60	0.83
9	6.90	74.50	9.26	8952	129743	6.90	2.36
10	4.15	54.70	7.59	9592	127893	7.50	0.09
11	4.65	69.00	6.74	10978	128543	8.40	1.66
12	5.40	59.00	9.15	10734	126284	8.50	0.65
13	4.25	54.75	7.76	10148	126856	8.00	0.24
14	4.75	43.00	11.05	11687	129853	9.00	2.05
15	4.15	50.15	8.28	11040	128368	8.60	0.32

The test method is to stop the belt every 10 minutes, record the value of the ore granularity detection system, unload the 1m long ore on the belt below the camera, and record the total weight and the weight on the screen after the manual screening. It can be seen from Table 2 that the manual screening data is between 5.00% and 11.05%, and the arithmetic average is 7.81%. The ore granularity detection system data is between 6.70% and 9.00%, and the arithmetic average is 7.83%. Although the actual data fluctuates greatly, if the average is compared over a long period of time, the data is relatively close.

The Root Mean Square Error (RMSE) can be represented by

$$e = \sqrt{\frac{1}{n}\sum_{k=1}^{n}\left|PA_k - PV_k\right|^2} \tag{5}$$

In the formula, n is the number of manual screenings, and $n = 15$ can be known from Table 2. PAk is the screening production, and PVk is the ore granularity detection system result.

Through the above analysis, it can be shown that the RMSE between the manual screening and ore granularity detection system is 1.2%, which proves that the system can accurately reflect the actual production of ore particle size distribution through image analysis and processing. It verifies the feasibility and the accuracy of the system.

5. Experiment and results

5.1. Experimental Steps and Parameters

The steps of ore granularity detection are shown in Fig. 3. The size of the ore flow image collected through the CCD industrial camera is 1920×1200. The camera model is osg230-150 um with 2.3 million pixels, 150 frames and USB 3.0. The dust on the site is relatively large, the camera is sealed in a protective box with high-light transmittance glass, which can prevent dust from entering or damaging the camera. The EC device is connected to the camera through USB3.0, and the specific configuration is: CPU core i74500U, memory 8GB, hard disk solid-state 128GB, USB × 4, LAN × 2, HDMI × 1, COM × 2, which supports the automatic power with win10 operating system and LabVIEW 2020 runtime. The IoT server of ThingsBoard and the HTTP server of Tomcat is deployed on the cloud. Both ThingsBoard and Tomcat are open-source applications, the former is used for data collection, processing, visualisation, and device management, whereas the latter is used for Java Servlet, JavaServer Pages, Java Expression Language and Java WebSocket technologies.

5.2. Experimental results

The real-time data and historical data of ore granularity data are shown in Fig. 2. It can be seen from the data on April 8, 2022, in Fig. 2, that the width of ore flow is maintained at about 400 mm all day. However, at 8 a.m., the ore break occurs, which will trigger the system alarm. As for the proportion of large blocks, it can be seen that most of the day the values stay below 10%, and the data rise to more than 12% around 0:00, 9:00, 11:00, 17:00 and 20:00, respectively. At this time, the system's abnormal ore size alarm will be triggered, and the data rises to more than 16% around 9:00 and 11:00. At this time, operators need to pay attention to whether the screen is damaged.

6. Discussion

Experimental results show that the proposed method can detect the ore granularity, ore flow width and ore flow terminal in real-time. Fig. 5(a) shows the image recognition results when the belt is full of ore. It can be seen that the ore granularity and ore flow width are correctly identified. Fig. 5(b) shows the result when the ore is partially loaded on the belt. Fig. 5(c) shows the result of identification when there is no ore on the belt. It can be seen from the above results that the proposed method in this paper can accurately identify the ore granularity and ore flow width for cases of full ores, partial ores, and no ore on the belt.

Machine vision has made a lot of achievements in identifying ore particle size in the mining industry. Although these studies can identify the ore granularity, there are also limitations. First,

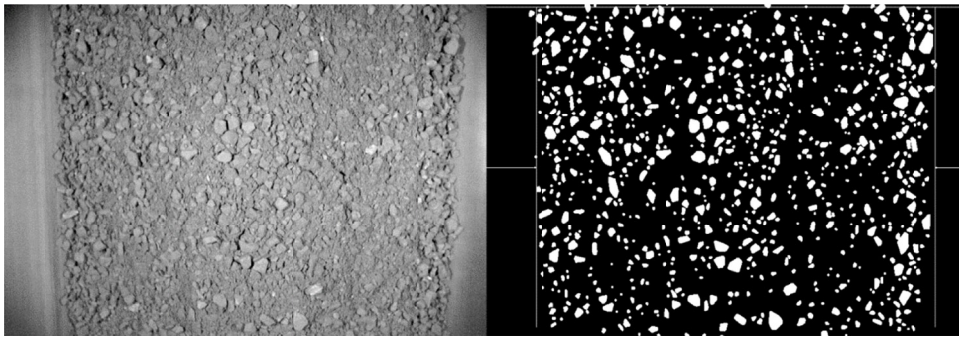

(a) Full ore identification

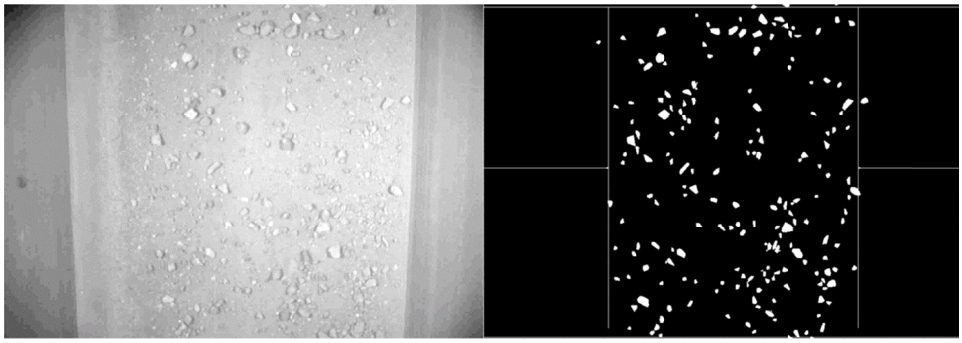

(b) Partial ore identification

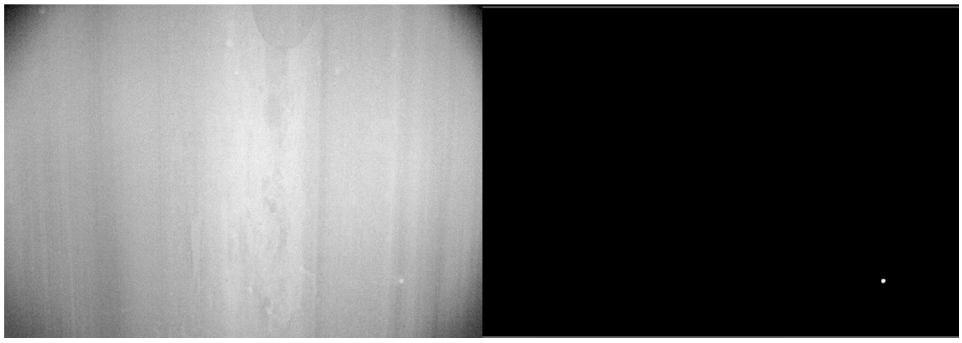

(c) Ore flow terminal identification

Fig. 5. Identify Results

the ore flow terminal cannot be detected in time and therefore, the alarm cannot be triggered in time. Second, it is not mentioned whether the upstream screen can be detected for breakage. Third, it did not mention whether historical and real-time data could be saved for big data analysis in the future. In a word, the method proposed in this paper can provide a reference for the staff to adjust the parameters of the crushing equipment, reduce the mechanical loss and the energy consumption of the equipment, improve the efficiency of crushing operation and reduce the failure rate of the crusher.

The limitations of this paper are as follows: First, there is a probability that the ore would be mixed with foreign material, including steel bars, angle iron, iron tools, etc. Considering the additional function is required for recognising foreign materials, the method of recognising ore granularity should be upgraded to add these functions as well. Second, because the ore surface is convex, different scale factors should be used from the middle to both sides of the image to further reduce the error. In summary, our next study is to combine the ore granularity and foreign object recognition algorithms and consider adopting different scale factors according to the distance between the camera and the ore surface.

7. Conclusions

Based on edge computing technology, an online detection method is investigated to accomplish ore granularity on high-speed conveyor belts rapidly and accurately, and the detection system utilising machine vision technology is designed in this paper. In the GUANBAOSHAN mine of Ansteel Group, the error between manual screening and image particle size analysis was studied. The accumulated error is below 1.2%. The main conclusions are as follows:

(1) The method proposed in this paper can meet the needs of particle size detection of high-speed belts in concentrators.
(2) The overall ore granularity data can be obtained from surface data.
(3) The edge computing device is used to process the collected image on site, and only the granularity data is output, changing the mode of uploading a large amount of image data to the server for processing.
(4) The obtained ore granularity data is helpful to optimise the crusher parameters and improve the ore crushing quality.

Based on the current research results, in the future, further in-depth research in the following two will be conducted:

(1) Combining the collected images with machine vision technology can integrate the foreign object recognition and belt deviation recognition functions, which will greatly improve the equipment safety and production efficiency of the concentrator.
(2) The ore surface is convex, different scale factors should be used from the middle to both sides of the image to further reduce the errors.

References

[1] L. Ma, Y. Zhang, G. Song, Z. Ma, T. Lu, In Ore Granularity Detection and Analysis System Based on Image Processing. 31st Chinese Control And Decision Conference (CCDC). Nanchang, Peoples R. China, Jun 03-05; Nanchang, Peoples R. China, 359-366 (2019). DOI: https://doi.org/10.1109/CCDC.2019.8832862

[2] J. Chen, H. Huang, A.G. Cohn, D. Zhang, M. Zhou, Machine learning-based classification of rock discontinuity trace: SMOTE oversampling integrated with GBT ensemble learning. International Journal Of Mining Science And Technology **32** (2), 309-322 (2022). DOI: https://doi.org/10.1016/j.ijmst.2021.08.004

[3] X. Li, L. Shen, Z. Ming, C. Zhang, H. Jiang, Laser-based on-line machine vision detection for longitudinal rip of conveyor belt. Optik **168**, 360-369 (2018). DOI: https://doi.org/10.1016/j.ijleo.2018.04.053.

[4] Y.M. Song, H. Ren, H.L. Xu, D. An, Experimental Study on Deformation and Damage Evolution of a Mining Roadway with Weak Layer Rock under Compression-shear Load. Archives of Mining Sciences **66** (3), 351-368 (2021). DOI: https://doi.org/10.24425/ams.2021.138593

[5] J. Zhou, J. Yu, Chisel edge wear measurement of high-speed steel twist drills based on machine vision. Computers In Industry **128**, 103436 (2021). DOI: https://doi.org/10.1016/j.compind.2021.103436

[6] M.T. Habib, A. Majumder, A.Z.M. Jakaria, M. Akter, M.S. Uddin, F. Ahmed, Machine vision based papaya disease recognition. Journal Of King Saud University-Computer And Information Sciences **32** (3), 300-309 (2020). DOI: https://doi.org/10.1016/j.jksuci.2018.06.006

[7] Z. Liu, B. Qu, Machine vision based online detection of PCB defect. Microprocessors and Microsystems **82**, 103807 (2021). DOI: https://doi.org/10.1016/j.micpro.2020.103807

[8] R.M.A. Eshaq, E. Hu, H.A.A.M. Qaid, Y. Zhang, T. Liu, Using Deep Convolutional Neural Networks and Infrared Thermography to Identify Coal Quality and Gangue. IEEE Access **9**, 147315-147327 (2021). DOI: https://doi.org/10.1109/ACCESS.2021.3121270

[9] Y. Guo, L. Chai, S.E. Aggrey, A. Oladeinde, J. Johnson, G. Zock, A Machine Vision-Based Method for Monitoring Broiler Chicken Floor Distribution. Sensors **20** (11), 3179 (2020). DOI: https://doi.org/10.3390/s20113179

[10] H. Tian, D. Wang, J. Lin, Q. Chen, Z. Liu, Surface Defects Detection of Stamping and Grinding Flat Parts Based on Machine Vision. Sensors **20** (16), 4531 (2020). DOI: https://doi.org/10.3390/s20164531

[11] H.M.A. Rashid, M. Ghazzali, U. Waqas, A.A. Malik, M.Z. Abubakar, Artificial Intelligence-Based Modeling for the Estimation Of Q-Factor and Elastic Young's Modulus of Sandstones Deteriorated by a Wetting-Drying Cyclic Process. Archives of Mining Sciences **66** (4), 635-658 (2021). DOI: https://doi.org/10.24425/ams.2021.138944

[12] S.K. Baduge, S. Thilakarathna, J.S. Perera, M. Arashpour, P. Sharafi, B. Teodosio, A. Shringi, P. Mendis, Artificial intelligence and smart vision for building and construction 4.0: Machine and deep learning methods and applications. Automation in Construction **141**, 104440 (2022). DOI: https://doi.org/10.1016/j.autcon.2022.104440

[13] C. Bhondayi, Flotation Froth Phase Bubble Size Measurement. Mineral Processing and Extractive Metallurgy Review **43** (2), 251-273 (2022). DOI: https://doi.org/10.1080/08827508.2020.1854250

[14] J. Maitre, K. Bouchard, L.P. Bedard, Mineral grains recognition using computer vision and machine learning. Computers & Geosciences **130**, 84-93 (2019). DOI: https://doi.org/10.1016/j.cageo.2019.05.009

[15] Z. Lu, X. Hu, Y. Lu, Particle Morphology Analysis of Biomass Material Based on Improved Image Processing Method. International Journal Of Analytical Chemistry **2017** (2017). DOI: https://doi.org/10.1155/2017/5840690

[16] A. Laucka, V. Adaskeviciute, D. Andriukaitis, Research of the Equipment Self-Calibration Methods for Different Shape Fertilizers Particles Distribution by Size Using Image Processing Measurement Method. Symmetry-Basel **11** (7), 838 (2019). DOI: https://doi.org/10.3390/sym11070838

[17] Z. Zhang, J. Yang, Online Analysis of Coal Ash Content on a Moving Conveyor Belt by Machine Vision. International Journal of Coal Preparation and Utilization **37** (2), 100-111 (2017). DOI: https://doi.org/10.1080/19392699.2016.1140650

[18] O.d.F. Martins Gomes, J.C. Alvarez Iglesias, S. Paciornik, M.B. Vieira, Classification of hematite types in iron ores through circularly polarized light microscopy and image analysis. Minerals Engineering **52**, 191-197 (2013). DOI: https://doi.org/10.1016/j.mineng.2013.07.019

[19] A. Heyduk, Elliptical shape and size approximation of a particle contour. IOP Conference Series: Earth and Environmental Science **261** (1), 012013 (2019). DOI: https://doi.org/10.1088/1755-1315/261/1/012013

[20] T. Thakur, A. Mehra, V. Hassija, V. Chamola, R. Srinivas, K.K. Gupta, A.P. Singh, Smart water conservation through a machine learning and blockchain-enabled decentralized edge computing network. Applied Soft Computing **106**, 107274 (2021). DOI: https://doi.org/10.1016/j.asoc.2021.107274

[21] M. Aazam, S. Zeadally, E.F. Flushing, Task offloading in edge computing for machine learning-based smart healthcare. Computer Networks **191**, 108019 (2021). DOI: https://doi.org/10.1016/j.comnet.2021.108019

[22] R. Rajavel, S.K. Ravichandran, K. Harimoorthy, P. Nagappan, K.R. Gobichettipalayam, IoT-based smart healthcare video surveillance system using edge computing. Journal of Ambient Intelligence and Humanized Computing **13** (6), 3195-3207 (2022). DOI: https://doi.org/10.1007/s12652-021-03157-1

[23] M. Gawas, H. Patil, S.S. Govekar, An integrative approach for secure data sharing in vehicular edge computing using Blockchain. Peer-To-Peer Networking and Applications **14** (5), 2840-2857 (2021). DOI: https://doi.org/10.1007/s12083-021-01107-4

[24] C. Li, X. Gao, S.L. Rowan, B. Hughes, W.A. Rogers, Measuring binary fluidization of nonspherical and spherical particles using machine learning aided image processing. AIChE Journal **68** (7), e17693 (2022). DOI: https://doi.org/10.1002/aic.17693

[25] X. Jia, Application of Planar Binary Image in Building Elevation Design. Scientific Programming **2022**, 9171941 (2022). DOI: https://doi.org/10.1155/2022/9171941

[26] K.T.N. Duarte, M.A.N. Moura, P.S. Martins, M.A.G.d. Carvalho, Brain Extraction in Multiple T1-weighted Magnetic Resonance Imaging slices using Digital Image Processing techniques. IEEE Latin America Transactions **20** (5), 831-838 (2022). DOI: https://doi.org/10.1109/TLA.2022.9693568

[27] D.S. Chéles, A.S. Ferreira, I.S. de Jesus, E.I. Fernandez, G.M. Pinheiro, E.A. Dal Molin, W. Alves, R.C.M. de Souza, L. Bori, M. Meseguer, J.C. Rocha, M.F.G. Nogueira, An Image Processing Protocol to Extract Variables Predictive of Human Embryo Fitness for Assisted Reproduction. Applied Sciences **12** (7), 3531 (2022). DOI: https://doi.org/10.3390/app12073531